

Article

Co-Exchange of Mn: A Simple Method to Improve Both the Hydrothermal Stability and Activity of Cu–SSZ-13 NH₃–SCR Catalysts

Chaoming Song¹, Lihong Zhang^{1,*} , Zhenguo Li^{2,3}, Yiren Lu^{4,*} and Kaixiang Li^{2,3}

¹ Department of Catalysis Science and Technology and Tianjin Key Laboratory of Applied Catalysis Science & Technology, School of Chemical Engineering and Technology, Tianjin University, Tianjin 300350, China; scm13303725721@sina.com

² Automotive Engineering Research Institute, China Automotive Technology and Research Center Co., Ltd., Tianjin 300300, China; lizhenguo@catarc.ac.cn (Z.L.); likaixiang@catarc.ac.cn (K.L.)

³ National Engineering Laboratory for Mobile Source Emission Control Technology, Tianjin 300300, China

⁴ School of Environmental Science and Engineering, Tianjin University, Tianjin 300072, China

* Correspondence: zlh_224@163.com (L.Z.); luyiren@tju.edu.cn (Y.L.)

Received: 24 April 2019; Accepted: 14 May 2019; Published: 17 May 2019



Abstract: A series of Cu–Mn–SSZ-13 catalysts were obtained by co-exchange of Mn and Cu into SSZ-13 together (ion exchange under a mixed solution of Cu(NO₃)₂ and Mn(NO₃)₂) and compared with Cu–SSZ-13 catalysts on the selective catalytic reduction (SCR) of nitric oxide (NO) by ammonia. The effects of total ion exchange degree and the effect of Mn species on the structure and performance of catalysts before and after hydrothermal aging were studied. All fresh and aged catalysts were characterized with several methods including temperature-programmed desorption with NH₃ (NH₃-TPD), X-ray diffraction (XRD), ²⁷Al and ²⁹Si solid-state nuclear magnetic resonance (NMR), scanning electron microscopy-energy dispersive spectroscopy (SEM-EDS) and low-temperature N₂ adsorption–desorption techniques. The results showed that the increase of the total ion exchange degree can reduce the content of residual Brønsted acid sites of catalysts, thus relieved the dealumination and the decrease of crystallinity of the catalyst during hydrothermal aging. The moderate addition of a Mn component in Cu–Mn–SSZ-13 catalysts significantly increased the activity of NO conversion at low temperature range. The selected Cu(0.2)Mn(0.1)–SSZ-13 catalyst achieved a high NO conversion of >90% in the wide and low temperature range of 175–525 °C and also exhibited good N₂ selectivity and excellent hydrothermal stability, which was related to the inhibition of the Mn component on the aggregation of Cu species and the pore destruction of the catalyst during hydrothermal aging.

Keywords: Selective catalytic reduction; nitric oxide; ammonia; SSZ-13; hydrothermal aging

1. Introduction

Nitrogen oxides (NO_x) emitted from mobile or stationary sources are among the major sources of air pollution, leading to a number of environmental problems such as photochemical smog and acid rain, which have great negative impacts on human health [1–5]. Owing to their negative environmental and health impacts, the removal of NO_x is becoming increasingly urgent. In addition to modifications made to combustion systems to reduce NO_x emissions, exhaust after-treatment technologies are required to meet stringent pollution control standards. In recent years, the selective catalytic reduction (SCR) of NO_x with NH₃ was proven to be an efficient method, regarded as one of the most promising candidates for NO_x reduction in flue gas [6–10].

A catalyst is one of the key components of an SCR system. Recently, the Cu-SSZ-13 catalyst with a Chabazite (CHA) structure—of which largest pore has an opening of 3.8 Å (eight-membered ring)—has gained attention owing to its high activity, stability, and selectivity [11–15]. The catalyst can maintain a high catalytic activity and excellent N₂ selectivity over a wide temperature range (250–550 °C), which is much better than the V-based and Cu-ZSM-5 catalysts [10,16]. However, this catalyst fails to meet the actual use conditions of diesel vehicles in the cold startup stage, which require better low-temperature activity [3,17,18]. Moreover, the vapor always emits from the lean combustion engine and the exhaust temperature can reach above 800 °C after diesel particulate filter (DPF) regeneration, thus the catalyst would undergo a high temperature hydrothermal aging process [19–21]. Therefore, it is necessary to improve the catalyst's low-temperature activity and its resistance to hydrothermal aging.

During the past years, many efforts have been made to solve these two problems. Steven et al. systematically studied the hydrothermal resistance of a commercial Cu-SSZ-13 catalyst and proposed a method for rapid hydrothermal aging. They found that the catalyst aged in the selected reactor aging conditions (800 °C) was comparable to the catalytic performance and characterization criteria of the 135,000-mile automotive aged catalyst [20]. In order to improve the hydrothermal stability of the catalyst, Gao. et al. introduced alkali metal ions and alkaline earth metal ions into the Cu-SSZ-13 catalyst, which had a notable effect due to the removal of the Brønsted (B) acid sites of the catalyst [22]. Meanwhile the mechanism of the hydrothermal aging of the catalyst has also attracted much attention. For example, Song et al. presented an atomic-level understanding of changes to the zeolite and the Cu active sites during hydrothermal aging and pointed out that the diffusion of Cu_xO_y clusters which is larger than the primary pore openings of SSZ-13 can be regarded as a primary cause for the structure damage of this catalyst [23]. As for the low-temperature activity, Liu et al. created a novel SCR catalyst with MnO_x-CeO₂ supported on Cu-SSZ-13 which reached an NO conversion efficiency of over 90% at 150 °C. Furthermore, they found that adding MnO_x-CeO₂ facilitated the conversion of bridging nitrate to monodentate nitrate, which might be the reason for the improved activity [24]. Meanwhile, considerable Mn-based and Ce-based oxide catalysts were investigated due to their excellent low-temperature SCR activities [25–28].

However, it is difficult to improve the catalyst's low-temperature activity and its resistance to hydrothermal aging simultaneously. Especially for the Cu-SSZ-13 catalyst, a high Cu ion exchange level is favorable for high activity at low temperature, while it is quite harmful to hydrothermal stability, so it is difficult to improve these two aspects by simply adjusting the Cu content [20,22,23]. By introducing Mn ions using the co-exchange method, we solve this problem ingeniously. Furthermore, most methods for increasing the low-temperature activity of the catalyst are accompanied by a decrease in the high-temperature activity [24,27,29]. Our method not only can improve the low-temperature activity but also can maintain the high-temperature activity stably. The novel Cu(0.2)Mn(0.1) catalyst can obtain over 90% NO conversion at 525 °C, which is equivalent to the high-temperature activity of the ordinary Cu-SSZ-13 catalysts. Meanwhile, the novel Cu(0.2)Mn(0.1) catalyst maintains a better performance than the ordinary Cu-SSZ-13 catalyst after hydrothermal aging. The wide temperature window and high hydrothermal stability meet the complex operating conditions and durability requirements of diesel engines, indicating broad application prospects and good business value.

2. Results and Discussion

2.1. Activity Test

The XRD curve and SEM images of synthetic SSZ-13 zeolite are shown in Figures S1 and S2. The result indicates the zeolite presents obvious CHA structural features [30,31].

Figure 1 shows the NH₃-SCR activity of these Cu-Mn catalysts. As the Mn/Cu ratio (in the mother liquid) rose from 0/10 to 4/10, the activity of the catalyst at low temperature increased and the temperature at NO conversion of 90% decreased from 225 to 175 °C. This indicates that the Cu-Mn catalysts obtained by co-exchange method can achieve good activity at both low and high

temperature. However, the Mn_xO_y -based, Mn_xO_y -modified or Mn_xO_y -SSZ-13 catalysts can only improve low-temperature NH_3 -SCR properties [24,25,32–34]. This is due to the fact that the Mn element here was introduced into the SSZ-13 zeolite in the form of stable and well-dispersed metal ions instead of big Mn_xO_y particles. The XRD results (Figure S3) shows that the Cu–Mn catalysts had the feature of the CHA structure. It was difficult to form the Mn_xO_y particles on the surface of Cu–Mn catalysts, since the concentration of the ionic solution used for exchange was quite dilute and the catalysts were rinsed by deionized water after exchange. However, the activity decreased when the Mn/Cu ratio reached 6/10 and the feature presented a seagull-shape showing an interesting phenomenon that from ~ 150 to ~ 250 °C the NO conversion decreased. This occurs when the gas hourly space velocity (GHSV) is relatively high [35,36], therefore, when the Mn/Cu ratio increased to 6/10, Mn ions competed with the Cu ions violently then the content of Cu ions decreased as shown in Table 1, which leads to an increase of relative GHSV.

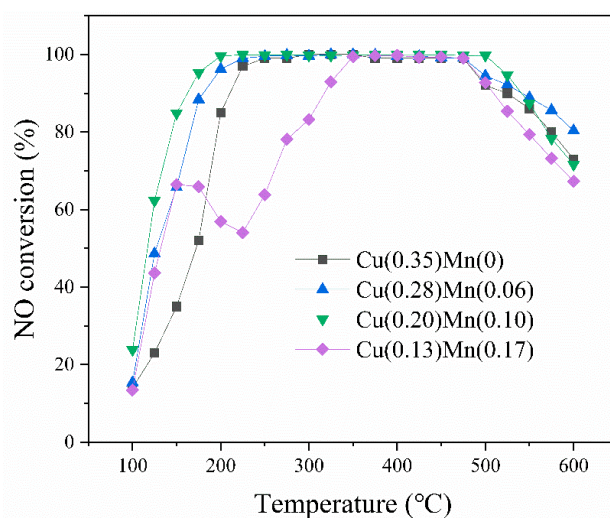


Figure 1. NO conversion of catalysts with different Mn/Cu ratios under a gas hourly space velocity (GHSV) of $30,000\text{ h}^{-1}$.

Table 1. Ion exchange degree of catalysts with different Mn/Cu molar ratios.

Mn/Cu Ratio	0/10	2/10	4/10	6/10
Ion Exchange Degree of Cu ^a	0.35	0.28	0.20	0.13
Ion Exchange Degree of Mn ^a	0	0.06	0.10	0.17

^a Ion exchange degree calculated from the equation of mol Cu (or Mn) $\times 2/\text{mol Al} \times 100\%$ based on the inductively coupled plasma atomic emission spectroscopy (ICP-AES) results.

In order to understand the effect of Mn species, we used Cu(0.2) and Cu(0.3) samples (with the same Cu content and the same total ion exchange degree as the Cu(0.2)Mn(0.1) catalyst) for comparison. It should be noted that it is difficult to obtain the exact same ion exchange degree or the same Cu content by the ion exchange method, so we used approximate processing.

The temperature programmed reduction with hydrogen (H_2 -TPR) curves given in Figure S4 show that the addition of Mn can make the reduction peak at ca. 220 °C enlarge and broaden due to the occurrence of shoulder peak at the side of high temperature. It indicates the addition of Mn species can interact with Cu ions and weak the interaction between Cu ions and the CHA framework. It is beneficial to the low-temperature SCR activity [22]. The formation of NO_2 from NO is a key step in standard SCR reactions [37]. The increase in the oxidizing ability of the catalyst made the reaction easier to occur and thereby increased the low temperature activity of the Cu–Mn catalyst. On the other hand, the introduction of Mn species by the co-exchange method caused an increase in the total ion exchange degree, leading to a decrease of the residual B acid sites, which are activity-silent [37–40]

and vulnerable during hydrothermal aging. Another important conclusion of this result is that the decrease of the residual B acid sites also can improve the stability of Cu–Mn catalyst [22,41].

From Figure 2a, we can see the Cu(0.2)Mn(0.1) catalyst presents the widest active temperature window. For the Cu(0.2) and Cu(0.3) samples, they were similar in activity at high temperatures and the Cu(0.3) catalyst had a higher activity in the low temperature range since it contained more active components. However, their activity in the low-temperature range was much lower than that of Cu(0.2)Mn(0.1), indicating that the increase of activity was not caused by the increase in ion exchange degree but was mainly caused by the promotion of Mn species. Compared with Figure 1 and the literature, we found that the temperature at which the seagull-like curve inflection appeared was different, meaning that the interaction between Cu and Mn changed the transition temperature [35,36]. This indicates that Cu^{2+} and Mn species interact with each other. The N_2 selectivity of all catalysts exceeded 95% throughout all of the temperature range, showing that this method not only increased activity, but also maintained high N_2 selectivity.

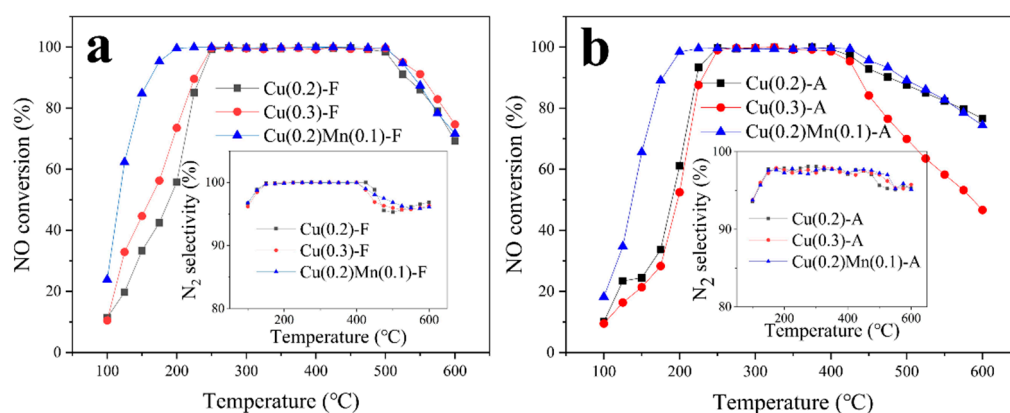


Figure 2. NO conversion with catalysts before (a) and after (b) hydrothermal aging under a GHSV of $30,000 \text{ h}^{-1}$.

Hydrothermal aging is one of the common reasons for the deactivation of NH_3 -SCR catalysts for diesel vehicles and it is important to evaluate the catalytic activity of catalysts after hydrothermal aging. Figure 2b is the activity curve of the catalysts after hydrothermal aging. As it shows, all the catalysts had varying degrees of deterioration compared with the fresh sample and the Cu(0.2)Mn(0.1) still possessed the best catalytic activity and maintained more than 90% NO conversion in the range of 180–475 °C. This indicates that it exhibits not only remarkable low temperature activity but also excellent hydrothermal stability, which is quite beneficial for the practical application of commercial SCR catalysts [42,43]. The Cu(0.3) catalyst had the most serious activity decrease, maintaining 90% NO conversion only between 250–425 °C. Furthermore, when the temperature was higher than 400 °C, all the catalysts NO conversion rate dropped sharply, while for fresh sample it needed 500 °C. The Cu(0.2) catalyst had a similar activity like the Cu(0.3) catalyst between 100 and 425 °C while it had a better performance in high-temperature range. This is due to the difference of NH_3 oxidation ability of catalysts and will be discussed in detail below. The N_2 selectivity of the three aged catalysts was slightly lower than that of the fresh samples, and the selectivity of the Cu(0.2)Mn(0.1) sample was the best which was consistent with the activity.

After hydrothermal aging the deterioration of the catalysts performance in high temperature was more serious than that in the low temperature section, which indicated that the catalyst activity in the high temperature section was more sensitive to hydrothermal aging. This is because during hydrothermal aging parts of active species translate from Cu^{2+} or $\text{Cu}(\text{OH})^+$ (two forms of Cu ions in the zeolite [44,45]) to Cu_xO_y [20,23]. These species have stronger oxidation than Cu ions and could oxidize the reducing agent NH_3 through the non-selective oxidation as shown in Formula (1), which is the main side reaction in SCR [31].



Since in the standard SCR process the NH_3 molecules and NO molecules are introduced at 1:1, the loss of reducing agent leads to a decrease in the NO conversion efficiency.

2.2. NH_3 and NO Oxidation Test

NH_3 oxidation capacity is an important indicator of SCR catalysts and the suitable oxidizability of the catalyst is pivotal to the SCR reaction [31,37,43,46]. Figure 3 shows the NH_3 oxidation performance curve of the three catalysts before and after hydrothermal aging. It can be seen from Figure 3a that all the catalysts had weak NH_3 oxidation ability below 200 °C and when the temperature was higher than 250 °C the oxidation capacity started to rise rapidly, both Cu^{2+} and $\text{Cu}(\text{OH})^+$ had a weak ability to oxidize NH_3 to N_2 at low temperatures [11]. As the temperature increased, the oxidation rate of NH_3 rose continuously and reached 100% at 450 °C. The $\text{Cu}(0.2)\text{Mn}(0.1)$ and $\text{Cu}(0.2)$ catalysts had very similar oxidation activities, meaning that the Mn introduced by the co-exchange method did not cause excessive oxidation of NH_3 . Comparing Figure 3a,b, we can see that the catalysts' NH_3 oxidation ability increased after hydrothermal aging. Too high of an NH_3 oxidation capacity leads to non-selective oxidation of reducing NH_3 , which is a major cause of reduced activity [20]. Among the samples, the $\text{Cu}(0.3)$ sample had the highest NH_3 oxidation promotion, indicating that samples with a high Cu content generated the most Cu_xO_y species during hydrothermal aging, leading to a higher oxidation ability [20,23,32,47]. This is the reason why the $\text{Cu}(0.3)$ catalyst performed the worst after hydrothermal aging, especially in the high temperature range.

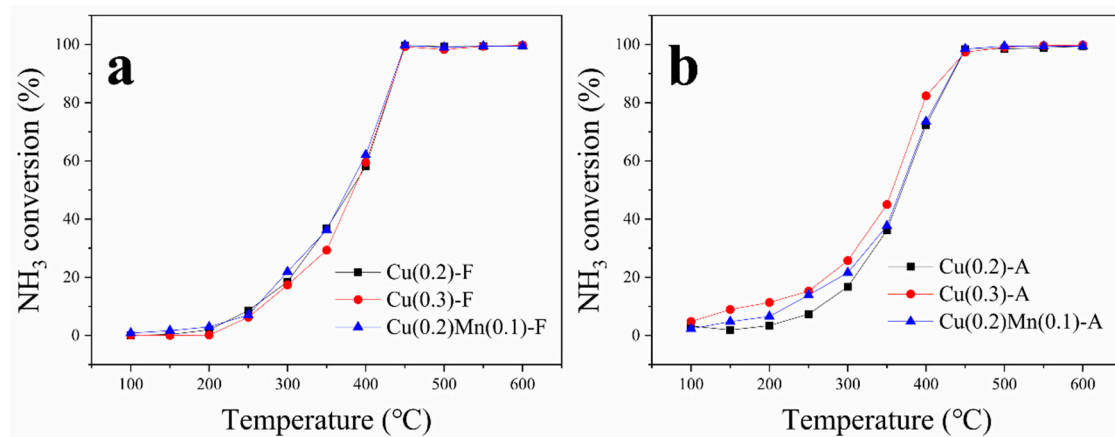


Figure 3. NH_3 oxidation of catalysts before (a) and after (b) hydrothermal aging under a GHSV of $30,000 \text{ h}^{-1}$.

NO oxidation is also relevant to better understand the SCR process [48,49]. As previously reported, isolated Cu species do not catalyze NO oxidation at low temperatures and NO oxidation only occurs when relatively stable O-bridged Cu-dimers are formed [35,49]. Therefore, the oxidation activity of NO reflects the difficulty of forming Cu-dimers in the catalyst. Figure 4a,b shows the performance of NO oxidation of the three catalysts before and after hydrothermal aging. All the activity curves exhibited a volcanic-like shape [20,35]. With the increase of the temperature, the NO conversion rate rose to reach the highest at around 400 °C and then decreased. This is because when the temperature is higher than 400 °C, Cu ions lose their complex small molecules and reduce their migration ability, which is not conducive to the formation of Cu dimers [44,50]. Furthermore, Cu dimers are more readily formed when there are more Cu ions, thus the $\text{Cu}(0.3)$ sample had the highest NO oxidation capacity. Unlike for the NH_3 oxidation process, the $\text{Cu}(0.2)$ and $\text{Cu}(0.2)\text{Mn}(0.1)$ catalysts exhibited different catalytic activities in the NO oxidation reaction, though they had the same Cu content. This indicates that the addition of Mn species has an inhibitory effect on the migration of Cu ions to generate Cu dimers.

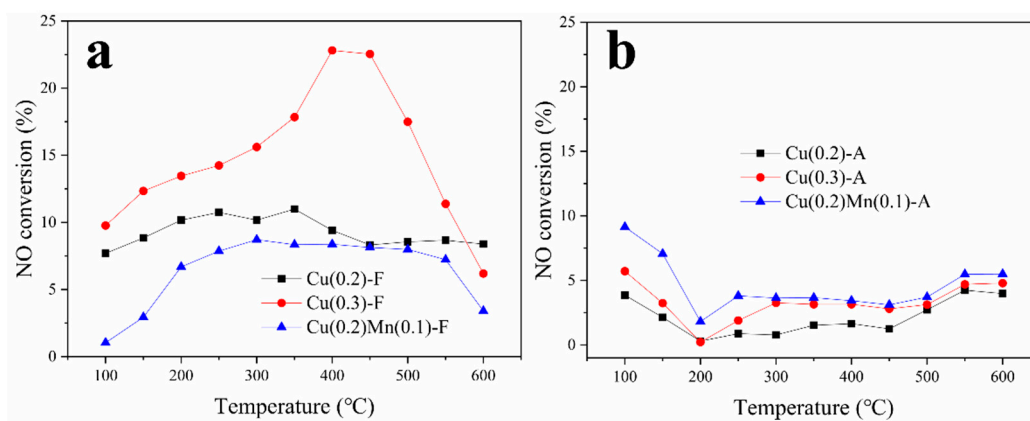


Figure 4. NO oxidation of catalysts before (a) and after (b) hydrothermal aging under a GHSV of 30,000 h⁻¹.

One possible way to enhance the SCR activity at low temperatures is to oxidize some of the NO to NO₂ so that a fast SCR occurs [47]. The reaction equation is presented below:



Our experiment proves that the introduction of Mn species by the co-exchange method in increasing the low-temperature activity of the catalyst does not follow the above mechanism and it was mainly caused by the promotion of Mn species. Figure 4b shows the ability of the catalysts to catalyze the oxidation of NO was greatly decreased after hydrothermal aging. As discussed above, some of the isolated Cu²⁺ or Cu(OH)⁺ species translate into Cu_xO_y, thus reducing the ability of catalysts to catalyze the oxidation of NO. Furthermore, the change of the NO oxidation capacity of the Cu(0.2)Mn(0.1) catalyst after hydrothermal aging was minimal, which also indicates that this catalyst had the best resistance to hydrothermal aging.

2.3. Temperature-Programmed Desorption with NH₃ (NH₃-TPD)

Hydrothermal aging can seriously affect the acidity of the catalysts, which is an important factor affecting catalytic performance [48]. NH₃-TPD experiments are often used to study the acidity of SSZ-13-based catalysts [38,44]. Figure 5 shows the NH₃ desorption profiles of the samples before and after hydrothermal aging. The fresh samples show the presence of three desorption peaks, centered at about 150 °C (low temperature, LT), 300 °C (intermediate temperature, IT), and 475 °C (high temperature, HT). The LT peak corresponding to the weak adsorption of NH₃ is assigned to physically adsorbed NH₃ and NH₃ adsorbed on weak acid sites [31,40,51]. The IT peak is attributed to NH₃ desorption from Lewis (L) acid sites and the HT peak is due to strongly bound NH₃, arising from protonated NH₃ formed over the B acid sites [31,44,52]. Notably, the Cu(0.3) and the Cu(0.2)Mn(0.1) samples presented similar NH₃-TPD curves and the areas of every peak were also substantially uniform. This is because they have the same total ion exchange degree, so they have the same L acid sites. (the L sites are generated by metal elements entering the zeolite via the co-exchange method [44]) This also indicates that the adsorption strength of NH₃ on Cu sites and Mn sites are similar. As for the Cu(0.2) sample, it was clear that the IT peak was smaller than that of others while the HT peak was a little bigger, as this sample had the lowest ion exchange degree. The LT peak areas of the three fresh samples were almost identical since they all had the same structure.

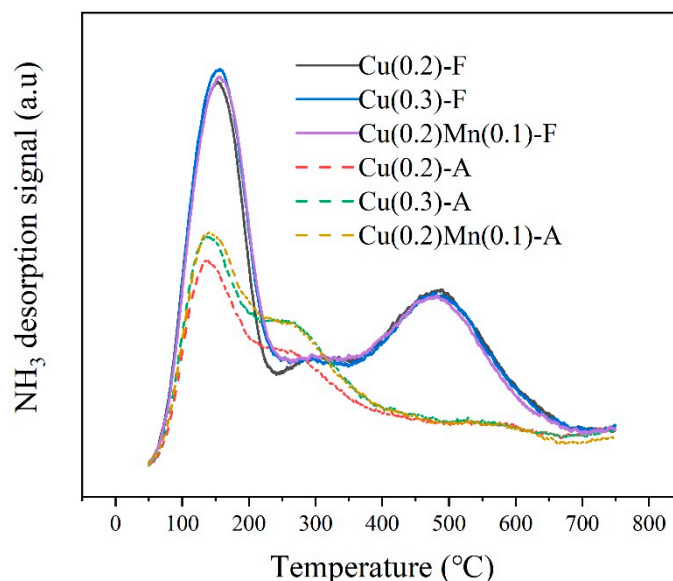


Figure 5. Temperature-programmed desorption with NH_3 (NH_3 -TPD) curves of catalysts before and after hydrothermal aging.

After hydrothermal aging, the NH_3 adsorption capacity was greatly decreased and the desorption peaks at different temperatures were various. All the LT peaks had a reduced area, which indicates that the structure of the catalysts was damaged during the hydrothermal aging. The area reduction of the Cu(0.2) sample was the most obvious, indicating that its damage was the most serious. The peaks in the HT range almost completely disappeared, revealing the fact that the B acid sites are the most vulnerable during the hydrothermal aging [22]. Meanwhile, the destruction of B acid sites causes a chain reaction that leads to the damage of the catalysts [23,53]. Thus, this influence can be effectively improved by increasing the amount of ion exchange to reduce the amount of residual B acid sites. It is interesting to note that the amount of NH_3 adsorbed at the IT segment increased. As mentioned above, Cu species change during hydrothermal aging. In addition to some of the isolate Cu species being converted to Cu_xO_y clusters, some of the $\text{Cu}(\text{OH})^+$ specie were converted to Cu^{2+} specie by the following equation:



This is because Cu species move to more thermodynamically stable sites at high temperatures [44,50,52]. At the same time, the curve of the Cu(0.2)Mn(0.1) sample was similar to that of the Cu(0.3) sample, which suggests that the Mn species may also move to more thermodynamically stable sites at high temperatures, although more experiments are needed to clearly illustrate this problem. In summary, by the co-exchange method, increasing the total ion exchange degree can slow down the destruction of the acidity and structure.

2.4. XRD

In order to illustrate the changes of phase of the three catalysts before and after hydrothermal aging, their XRD patterns are shown in Figure 6. From Figure 6a, it can be seen that the XRD patterns of these fresh samples are similar to those reported in the literature for SSZ-13 materials [54]. The CHA phase (JCPDS file No.47-0762) was observed as the only crystalline phase in all samples. In each case, the diffraction intensities of the CHA phase of all samples had no difference. This indicates that the introduction of a small number of Cu and Mn elements does not influence the host structure. However, there was an obvious decrease of the diffraction intensities of the CHA phase for aged samples. This indicates that the crystal phase of the catalysts was damaged, resulting in a decrease in crystallinity. The maintained CHA phase can be used to explain the stable catalytic performance of NH_3 -SCR over

these catalysts. It should be noted that the degree of damage of the Cu(0.2) sample was more serious than that of Cu(0.2)Mn(0.1) and Cu(0.3) samples. This means that the total ion exchange degree has a great influence on the stability. As mentioned above this is because the B acid sites are susceptible to damage during hydrothermal aging, while the higher exchange degree means that more H⁺ sites in SSZ-13 can be replaced by metal ions, which effectively reduce the amount of residual B acid sites and enhance the stability of the catalysts [22,23,55].

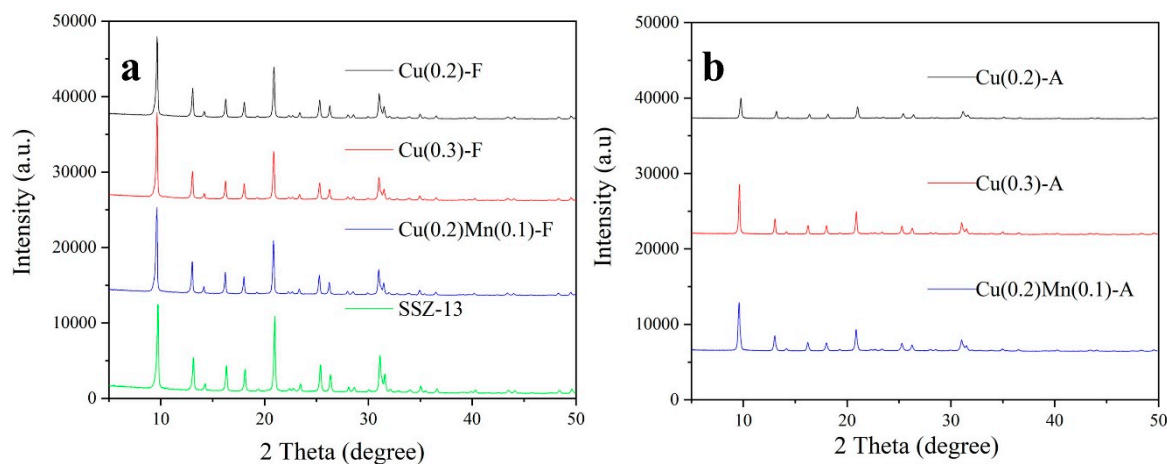


Figure 6. X-ray diffraction (XRD) patterns of catalysts before (a) and after (b) hydrothermal aging.

2.5. NMR

NMR is a commonly used method to characterize the changes in a zeolite framework structure. Figure 7a displays the ²⁷Al NMR spectra acquired from hydrated, ambient samples before and after hydrothermal aging; the corresponding ²⁹Si NMR spectra are presented in Figure 7b. The features appearing at 58 ppm are attributed to the framework Al (Alf) and the features appearing at 0 ppm are attributed to the extra framework Al (EFAI) [53,56,57]. EFAI also has a certain catalytic activity and it can be seen from the spectrum that all three fresh samples contained almost no EFAI, thus eliminating the effect of the EFAI on the catalyst [40]. This is because the zeolite used in our experiments had a relatively high Si/Al ratio (20), which is less prone to generate EFAI [48,56]. After hydrothermal aging, the Alf of every sample greatly decreased and the corresponding EFAI slightly increased, indicating that the dealumination of the zeolite skeleton occurred during hydrothermal aging—one of the main reasons leading to the destruction of the zeolite. Note that the reduction of the Alf was much larger than the increase of the EFAI. This is because some of Al can be converted to NMR-silent species [23,45,58]. Since the acidity of the zeolite is caused by the coordination imbalance of Al and O atoms, the loss of this portion of Al can result in a decrease in the total acidity of the zeolite. This is consistent with the NH₃-TPD results. Among the three aged samples, the Alf of the Cu(0.2) was the most severely decreased while the changes of the Cu(0.3) and the Cu(0.2)Mn(0.1) samples were much slighter. This is similar to the result of XRD and it means that increasing the total ion exchange degree of the zeolite can reduce the dealumination of the zeolite. The ²⁹Si NMR spectra show the same result. The features appearing at −111 ppm are attributed to Si(4Si, 0Al) and the features appearing at −105 ppm are attributed to Si(3Si, 1Al) [53,56,57]. After hydrothermal aging, the −105 ppm feature declined while the −111 ppm feature rose, consistent with catalyst dealumination. It is clear that the Cu(0.2) sample had the most obvious change in peak intensity, also indicating that the degree of total ion exchange has an important influence on the structural stability of the catalysts.

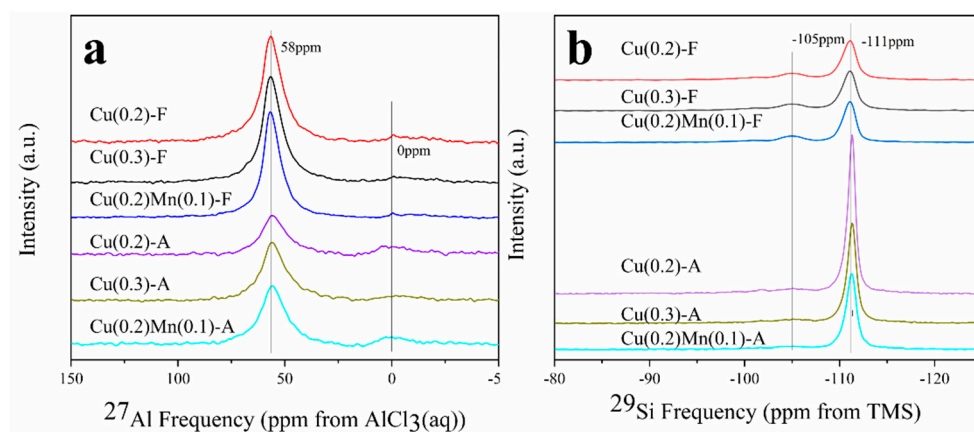


Figure 7. Solid-state ^{27}Al -NMR spectra of the samples of catalysts before and after hydrothermal aging (a) and solid-state ^{29}Si -NMR spectra of the samples of catalysts before and after hydrothermal aging (b).

From the discussion above, it can be seen that the total ion exchange plays an important role in the hydrothermal aging process of the catalyst. The content of residual B acid sites in the catalyst can be decreased, thus the acidity and structural damage of the catalyst during hydrothermal aging can be effectively reduced by increasing the total ion exchange degree of the catalysts. However, simply increasing the content of Cu^{2+} to increase the total ion exchange degree makes the catalyst prone to creating Cu_xO_y species, as shown in the NH_3 oxidation experiment, which leads to non-selective reduction reactions. Meanwhile, simply increasing the content of Cu^{2+} leads to the damage of the catalyst's pores during hydrothermal aging and this will be discussed in detail below.

2.6. Physical Properties

Figure 8 shows the SEM images of the fresh and aged samples. The fresh samples exhibited a cube shape, which is the typical morphology of SSZ-13 and the average particle size of the catalyst was about 200 nm. In addition, the images indicate that the catalysts showed a perfect degree of crystallization which is in accordance with the XRD results. After hydrothermal aging, most of the particles still retained the structure of the cube. That means that the structure of the catalysts was partially destroyed after hydrothermal aging while its basic structure could be maintained and this consistent with our findings above. It is clear from the mapping pictures shown in Figure S5 that the Cu element and Mn element of the Cu(0.2)Mn(0.1) sample were quite evenly distributed.

Figure 9 depicts the curves of the micropores and mesopores before and after the hydrothermal aging of the catalysts. In the micropores (diameter <2 nm), as Figure 9a,c,e show, the pores of the samples were concentrated at about 0.38 nm, which is a perfect reflection of the theoretical pore size of the CHA zeolite. It can be seen that after hydrothermal aging, the Cu(0.3) sample suffered the largest reduction of microporous pores, while the Cu(0.2)Mn(0.1) sample exhibited the least reduction. Meanwhile, as shown in the mesoporous portion, the amount of mesopores (2~50 nm as shown in Figure 9b,d,f) increased after hydrothermal aging. Consistent with the change of micropores, the increase of the mesopores of the Cu(0.3) sample was the largest while there was almost no difference in the mesopores of the Cu(0.2)Mn(0.1) sample. This is also important evidence for the pore destruction of the catalysts.

The destruction of the pore structure of the catalyst is due to the formation and migration of Cu_xO_y , with a larger than the primary pore size (0.38 nm) of SSZ-13 [23]. The results indicate that addition of Mn species can slow down the formation of Cu_xO_y and alleviate the damage of the pore structure of the catalysts. The Brunauer–Emmett–Teller (BET) specific surface area embedded in Figure 9 also reflects the extent to which the catalysts were affected by hydrothermal aging. All the samples before hydrothermal aging had similar specific surface areas and their slight differences may have been due to subtle differences in the preparation process. After hydrothermal aging, the specific surface area of

the Cu(0.2)Mn(0.1) was the largest, and that of the Cu(0.3) was the smallest also revealing that the addition of Mn species greatly slowed down the damage of the catalyst during hydrothermal aging.

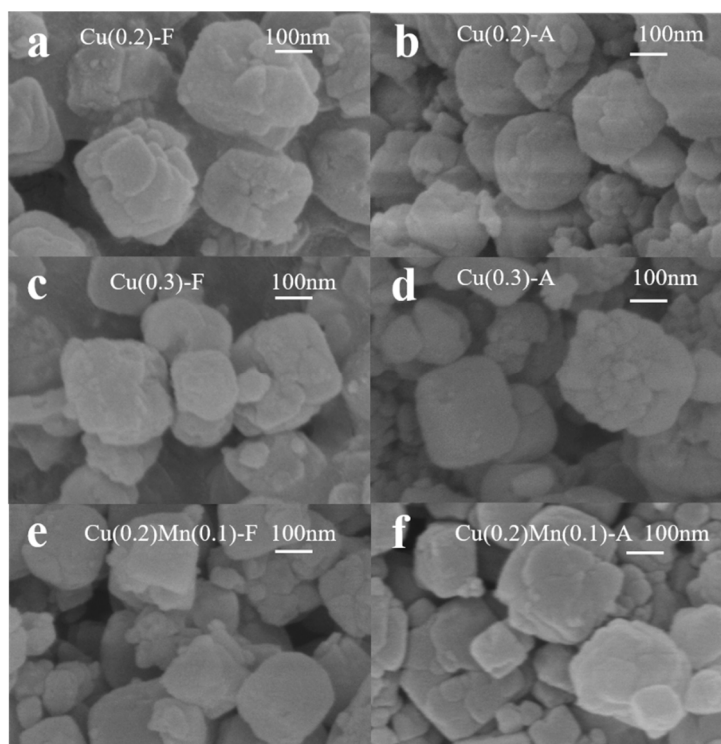


Figure 8. SEM images of catalysts before (a,c,e) and after (b,d,f) hydrothermal aging.

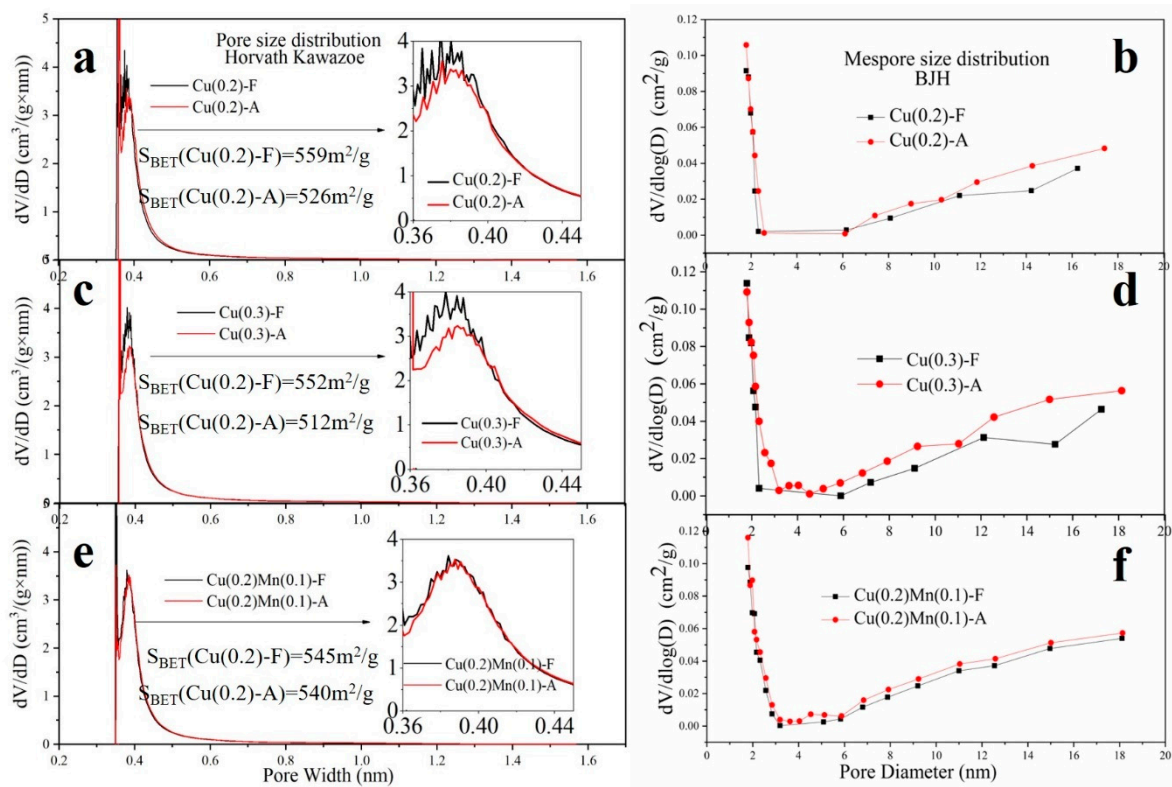


Figure 9. Micropore size distributions of catalysts before and after hydrothermal aging (a,c,e) and mesopore size distributions before and after hydrothermal aging (b,d,f).

3. Materials and Methods

3.1. Catalyst Preparation

The SSZ-13 zeolite was prepared using a hydrothermal method with the N, N, N-trimethyl-1-1-adamantammonium hydroxide (TMAdaOH) serving as a structure-directing agent (SDA). Firstly, 4 g of NaAlO₂ and 0.2 g NaOH were added to 20 g of deionized water and the mixture was stirred at room temperature for 30 min. Then 6 g SDA was added to the solution and 20 g of silica sol (40%) was added dropwise with constant stirring. After stirring for 4 h, the sol was transferred into Teflon-lined autoclaves and reacted at 160 °C for 96 h. After that, the product was separated from the mother liquid via centrifugation and washing with deionized water three times. Finally, the solid powder was dried overnight at 120 °C, then calcined at 390 °C for 1 hour and then heated at 2 °C/min to 550 °C and held for 6 h.

The Cu–SSZ-13 catalysts were prepared using a standard two-step solution ion exchange method. First, the obtained Na–SSZ-13 was exchanged three times with a 0.1 M solution of NH₄NO₃ at 80 °C for 12 h to generate the NH₄–SSZ-13. Then the Cu–SSZ-13 was obtained by exchanging with a 0.1 M solution of Cu(NO₃)₂ and the pH of the solution was adjusted to 3 by adding dilute HNO₃ solution (10%). Similarly, Cu–Mn–SSZ-13 samples with different Mn/Cu ratios were prepared by ion exchange under a mixed solution of Cu(NO₃)₂ and Mn(NO₃)₂ (co-exchange method). By changing the Mn/Cu ratio in the solution, Cu–Mn–SSZ-13 catalysts with different ion exchange degrees were obtained and the content of Cu and Mn was measured by inductively coupled plasma atomic emission spectroscopy (ICP-AES). The ion exchange degree was calculated by Formula 5 and the results are shown in Table 1, at the same time, the Si/Al molar ratio of all samples was 20. Finally, all the solid powders were calcined in air at 550 °C for 6 h.

$$\text{ion exchange degree} = \left(\frac{\text{mole Cu (or Mn)}}{\text{mole Al}} \right) \times 200\% \quad (5)$$

The Cu–Mn–SSZ-13 samples with different molar ratio of Mn/Cu catalysts were named as Cu(x)Mn(y)-F(A), in which x and y represents the ion exchange degree of Cu and Mn elements, and fresh or hydrothermally aged samples were distinguished by the suffix letter F or A

3.2. Catalyst Characterization

The catalyst structures were characterized by powder X-ray diffraction (XRD) on a Rigaku D/MAX 2550 diffractometer (Karlsruhe, Germany) equipped with Cu K α (40 kV, 40 mA) radiation ($\lambda = 1.540598 \text{ \AA}$) using a scan range from 5 to 50° with a scan step of 8° min⁻¹.

The element contents were determined by inductively coupled plasma atomic emission spectroscopy (ICP-AES) (Massachusetts, USA).

Temperature programmed reduction with hydrogen (H₂-TPR) experiments were performed on a Micromeritics Auto Chem II chemisorption analyzer (Norcross, USA). In each experiment, 100 mg of sample was loaded into a quartz reactor and then pretreated in He (50 mL/min) at 400 °C for 2 h. The reduction of the sample was carried out from 50 °C to 600 °C under a flow of 10% H₂/Ar (50 mL/min) at 10 °C/min.

Low-temperature N₂ adsorption–desorption analysis was carried out at 77 K using a Micromeritics ASAP 2460 instrument (Norcross, USA). Before the measurement, all samples were dried overnight at 120 °C, then treated under vacuum at 90 °C for 3 h and finally treated under vacuum at 250 °C for 6 h. The specific surface area, mesoporous and micropore size were determined by the Brunauer–Emmett–Teller (BET) method, Barrett–Joyner–Halenda (BJH) method and Horvath–Kawazoe (H–K) method, respectively.

Temperature programmed desorption with NH₃ (NH₃-TPD) tests were conducted on a Micromeritics Auto Chem II chemisorption analyzer (Norcross, USA). The powder samples were about 100 mg and before testing the powder samples needed to be pre-treated with He for 2 h at 400 °C, then

cooled to 50 °C. After that, the samples were exposed to 2% NH₃/He for 2 h at 50 °C, followed by a purge in He at 50 °C for 2 h. Finally, the TPD data were obtained by heating the samples from 50 °C to 750 °C with a heating rate of 10 °C/min under pure He (100 mL/min).

Solid-state nuclear magnetic resonance (NMR) analysis of the samples was conducted on an Infinityplus 300 instrument (California, USA). About 0.1 g of the samples were transferred into a gastight rotor, and the rotor mounted into the NMR spectrometer. ²⁷Al chemical shifts were reported relative to a 0.1 M aqueous AlCl₃ solution and ²⁹Si chemical shifts were reported relative to a Si(CH₃)₄ standard.

Scanning electron microscopy (SEM) and energy dispersive spectroscopy (EDS) was carried out on Hitachi S-4800 instrument (Tokyo, Japan) using a 3.0 kV electron beam and before test, all samples were sprayed with gold for 50 s.

3.3. Catalytic Activity and Hydrothermal Stability Measurements

NH₃-SCR experiments were performed in a fixed bed reactor with a 12 mm inner diameter. The catalysts were crushed and sieved into 40–60 mesh before the catalytic measurements. The reaction conditions were 500 ppm NO, 500 ppm NH₃, 5 vol% O₂, 2.5 vol% H₂O, and the gas hourly space velocity (GHSV) = 30,000 h⁻¹. The concentrations of NH₃, NO, NO₂, and N₂O were measured by a Fourier-transform infrared (FTIR) spectrometer (Thermo Nicolet IS 10).

The NH₃ and NO oxidation reactions were also conducted under the same conditions except that, in NH₃ oxidation, the NO feed was stopped while in the NO oxidation, the NH₃ feed was stopped.

The hydrothermal aging experiment was carried out in a vacuum tube furnace. The aging gas components included 75% N₂, 15% O₂ and 10% H₂O. The aging temperature was 800 °C and the GHSV = 30,000 h⁻¹.

The conversion of NO and NH₃ and the selectivity of N₂ were calculated by the following equations:

$$\text{NO conversion} = \left(1 - \frac{\text{NO}_{\text{outlet}}}{\text{NO}_{\text{inlet}}}\right) \times 100\% \quad (6)$$

$$\text{NH}_3 \text{ conversion} = \left(1 - \frac{\text{NH}_3_{\text{outlet}}}{\text{NH}_3_{\text{inlet}}}\right) \times 100\% \quad (7)$$

$$\text{N}_2 \text{ selectivity} = \frac{\text{NH}_3_{\text{inlet}} + \text{NO}_{\text{inlet}} - \text{NH}_3_{\text{outlet}} - \text{NO}_{\text{outlet}} - 2\text{N}_2\text{O}_{\text{outlet}} - \text{NO}_2_{\text{outlet}}}{\text{NH}_3_{\text{inlet}} + \text{NO}_{\text{inlet}} - \text{NH}_3_{\text{outlet}} - \text{NO}_{\text{outlet}}} \times 100\%. \quad (8)$$

4. Conclusions

In our study, it was found that Mn was a promising promoter and changed the structure, stability and performance of Cu-SSZ-13 catalysts. Therefore, some points can be put forward as follows:

(1) Several Cu-Mn-SSZ-13 catalysts with different Mn/Cu molar ratio and well-crystallized SSZ-13 CHA structure were prepared by ion-exchange of Mn and Cu into SSZ-13 together.

(2) The Cu(0.2)Mn(0.1)-SSZ-13 catalyst has high reactivity at low-temperature and strong resistance to hydrothermal aging. It presents a more than 90% NO conversion in a wide temperature range (175–525 °C) and can still maintain more than 90% NO conversion in a temperature range of 180–475 °C after rigorous hydrothermal aging.

(3) The high total ion exchange degree is beneficial in reducing the residual B acid sites and thus decreasing the destruction of SSZ-13 phase and inhibiting the dealumination of the skeleton during the hydrothermal process.

(4) The moderate addition of Mn to Cu-SSZ-13 contribute to the high NH₃-SCR activity and inhibits the aggregation of Cu species and the pore destruction of the catalyst during hydrothermal aging thus achieving excellent hydrothermal stability.

Supplementary Materials: The following are available online <http://www.mdpi.com/2073-4344/9/5/455/s1>, Figure S1: XRD pattern of the synthetic SSZ-13 powder, Figure S2: SEM images of the synthetic SSZ-13 powder, Figure S3: XRD patterns of different Cu-Mn-SSZ-13 catalysts, Figure S4: Temperature programmed

reduction with hydrogen (H₂-TPR) curves of different Cu–Mn–SSZ-13 catalysts, Figure S5: Elemental mapping images of fresh and aged Cu(0.2)Mn(0.1) catalysts.

Author Contributions: C.S. and Y.L. conceived and designed the experiments; C.S., Z.L. and K.L. performed the experiments and contributed reagents and materials; C.S. wrote the manuscript; L.Z. and Y.L. checked and corrected the manuscript.

Funding: This research was funded by National Natural Science Foundation of China grant number [21776214].

Conflicts of Interest: The authors declare no conflict of interest.

References

1. Zhang, R.; Liu, N.; Lei, Z.; Chen, B. Selective Transformation of Various Nitrogen-Containing Exhaust Gases toward N₂ over Zeolite Catalysts. *Chem. Rev.* **2016**, *116*, 3658–3721. [[CrossRef](#)]
2. Ruggeri, M.P.; Luo, J.; Nova, I.; Tronconi, E.; Kamasamudram, K.; Yezerets, A. Novel method of ammonium nitrate quantification in SCR catalysts. *Catal. Today* **2018**, *307*, 48–54. [[CrossRef](#)]
3. Xu, J.; Chen, G.; Guo, F.; Xie, J. Development of wide-temperature vanadium-based catalysts for selective catalytic reducing of NO_x with ammonia: Review. *Chem. Eng. J.* **2018**, *353*, 507–518. [[CrossRef](#)]
4. Hammershøj, P.S.; Jangjou, Y.; Epling, W.S.; Jensen, A.D.; Janssens, T.V.W. Reversible and irreversible deactivation of Cu-CHA NH₃-SCR catalysts by SO₂ and SO₃. *Appl. Catal. B Environ.* **2018**, *226*, 38–45. [[CrossRef](#)]
5. Beale, A.M.; Gao, F.; Lezcano-Gonzalez, I.; Peden, C.H.F.; Szanyi, J. Recent advances in automotive catalysis for NO_x emission control by small-pore microporous materials. *Chem. Soc. Rev.* **2015**, *44*, 7371–7405. [[CrossRef](#)]
6. Xin, Y.; Li, Q.; Zhang, Z. Zeolitic Materials for DeNO_x Selective Catalytic Reduction. *ChemCatChem* **2018**, *10*, 29–41. [[CrossRef](#)]
7. Clemens, A.K.S.; Shishkin, A.; Carlsson, P.A.; Skoglundh, M.; Martínez-Casado, F.J.; Matěj, Z.; Balmes, O.; Härelind, H. Reaction-driven Ion Exchange of Copper into Zeolite SSZ-13. *ACS Catal.* **2015**, *5*, 6209–6218. [[CrossRef](#)]
8. Borfecchia, E.; Beato, P.; Svelle, S.; Olsbye, U.; Lamberti, C.; Bordiga, S. Cu-CHA—A model system for applied selective redox catalysis. *Chem. Soc. Rev.* **2018**, *47*, 8097–8133. [[CrossRef](#)]
9. Wijayanti, K.; Xie, K.; Kumar, A.; Kamasamudram, K.; Olsson, L. Effect of gas compositions on SO₂ poisoning over Cu/SSZ-13 used for NH₃-SCR. *Appl. Catal. B Environ.* **2017**, *219*, 142–154. [[CrossRef](#)]
10. Granger, P.; Parvulescu, V.I. Catalytic NO_x Abatement Systems for Mobile Sources: From Three-Way to Lean Burn after-Treatment Technologies. *Chem. Rev.* **2011**, *111*, 3155–3207. [[CrossRef](#)]
11. Gao, F.; Walter, E.D.; Karp, E.M.; Luo, J.; Tonkyn, R.G.; Kwak, J.H.; Szanyi, J.; Peden, C.H.F. Structure–activity relationships in NH₃-SCR over Cu-SSZ-13 as probed by reaction kinetics and EPR studies. *J. Catal.* **2013**, *300*, 20–29. [[CrossRef](#)]
12. Schmidt, J.E.; Oord, R.; Guo, W.; Poplawsky, J.D.; Weckhuysen, B.M. Nanoscale tomography reveals the deactivation of automotive copper-exchanged zeolite catalysts. *Nat. Commun.* **2017**, *8*, 1666. [[CrossRef](#)]
13. Marberger, A.; Petrov, A.W.; Steiger, P.; Elsener, M.; Kröcher, O.; Nachttegaal, M.; Ferri, D. Time-resolved copper speciation during selective catalytic reduction of NO on Cu-SSZ-13. *Nat. Catal.* **2018**, *1*, 221–227. [[CrossRef](#)]
14. Zhao, Z.; Yu, R.; Zhao, R.; Shi, C.; Gies, H.; Xiao, F.-S.; De Vos, D.; Yokoi, T.; Bao, X.; Kolb, U.; et al. Cu-exchanged Al-rich SSZ-13 zeolite from organotemplate-free synthesis as NH₃-SCR catalyst: Effects of Na⁺ ions on the activity and hydrothermal stability. *Appl. Catal. B Environ.* **2017**, *217*, 421–428. [[CrossRef](#)]
15. Jangjou, Y.; Do, Q.; Gu, Y.; Lim, L.-G.; Sun, H.; Wang, D.; Kumar, A.; Li, J.; Grabow, L.C.; Epling, W.S. Nature of Cu Active Centers in Cu-SSZ-13 and Their Responses to SO₂ Exposure. *ACS Catal.* **2018**, *8*, 1325–1337. [[CrossRef](#)]
16. Kwak, J.H.; Tonkyn, R.G.; Kim, D.H.; Szanyi, J.; Peden, C.H.F. Excellent activity and selectivity of Cu-SSZ-13 in the selective catalytic reduction of NO_x with NH₃. *J. Catal.* **2010**, *275*, 187–190. [[CrossRef](#)]
17. Forzatti, P.; Nova, I.; Tronconi, E. Enhanced NH₃ Selective Catalytic Reduction for NO_x Abatement. *Angew. Chem. Int. Ed.* **2009**, *48*, 8366–8368. [[CrossRef](#)]
18. Liu, C.; Shi, J.-W.; Gao, C.; Niu, C. Manganese oxide-based catalysts for low-temperature selective catalytic reduction of NO_x with NH₃: A review. *Appl. Catal. A Gen.* **2016**, *522*, 54–69. [[CrossRef](#)]
19. Wang, D.; Jangjou, Y.; Liu, Y.; Sharma, M.K.; Luo, J.; Li, J.; Kamasamudram, K.; Epling, W.S. A comparison of hydrothermal aging effects on NH₃-SCR of NO_x over Cu-SSZ-13 and Cu-SAPO-34 catalysts. *Appl. Catal. B Environ.* **2015**, *165*, 438–445. [[CrossRef](#)]

20. Schmiege, S.J.; Oh, S.H.; Kim, C.H.; Brown, D.B.; Lee, J.H.; Peden, C.H.F.; Kim, D.H. Thermal durability of Cu-CHA NH₃-SCR catalysts for diesel NO_x reduction. *Catal. Today* **2012**, *184*, 252–261. [[CrossRef](#)]
21. Kim, Y.J.; Lee, J.K.; Min, K.M.; Hong, S.B.; Nam, I.-S.; Cho, B.K. Hydrothermal stability of CuSSZ13 for reducing NO_x by NH₃. *J. Catal.* **2014**, *311*, 447–457. [[CrossRef](#)]
22. Gao, F.; Wang, Y.; Washton, N.M.; Kollár, M.; Szanyi, J.; Peden, C.H.F. Effects of Alkali and Alkaline Earth Cocations on the Activity and Hydrothermal Stability of Cu/SSZ-13 NH₃ -SCR Catalysts. *ACS Catal.* **2015**, *5*, 6780–6791. [[CrossRef](#)]
23. Song, J.; Wang, Y.; Walter, E.D.; Washton, N.M.; Mei, D.; Kovarik, L.; Engelhard, M.H.; Proding, S.; Wang, Y.; Peden, C.H.F.; et al. Toward Rational Design of Cu/SSZ-13 Selective Catalytic Reduction Catalysts: Implications from Atomic-Level Understanding of Hydrothermal Stability. *ACS Catal.* **2017**, *7*, 8214–8227. [[CrossRef](#)]
24. Liu, Q.; Fu, Z.; Ma, L.; Niu, H.; Liu, C.; Li, J.; Zhang, Z. MnO -CeO₂ supported on Cu-SSZ-13: A novel SCR catalyst in a wide temperature range. *Appl. Catal. A Gen.* **2017**, *547*, 146–154. [[CrossRef](#)]
25. Boningari, T.; Ettireddy, P.R.; Somogyvari, A.; Liu, Y.; Vorontsov, A.; McDonald, C.A.; Smirniotis, P.G. Influence of elevated surface texture hydrated titania on Ce-doped Mn/TiO₂ catalysts for the low-temperature SCR of NO_x under oxygen-rich conditions. *J. Catal.* **2015**, *325*, 145–155. [[CrossRef](#)]
26. Pappas, D.K.; Boningari, T.; Boolchand, P.; Smirniotis, P.G. Novel manganese oxide confined interweaved titania nanotubes for the low-temperature Selective Catalytic Reduction (SCR) of NO_x by NH₃. *J. Catal.* **2016**, *334*, 1–13. [[CrossRef](#)]
27. Meng, D.; Xu, Q.; Jiao, Y.; Guo, Y.; Guo, Y.; Wang, L.; Lu, G.; Zhan, W. Spinel structured Co_aMn_bO_x mixed oxide catalyst for the selective catalytic reduction of NO_x with NH₃. *Appl. Catal. B Environ.* **2018**, *221*, 652–663. [[CrossRef](#)]
28. Shen, Q.; Zhang, L.; Sun, N.; Wang, H.; Zhong, L.; He, C.; Wei, W.; Sun, Y. Hollow MnO_x-CeO₂ mixed oxides as highly efficient catalysts in NO oxidation. *Chem. Eng. J.* **2017**, *322*, 46–55. [[CrossRef](#)]
29. Cheng, M.; Jiang, B.; Yao, S.; Han, J.; Zhao, S.; Tang, X.; Zhang, J.; Wang, T. Mechanism of NH₃ Selective Catalytic Reduction Reaction for NO_x Removal from Diesel Engine Exhaust and Hydrothermal Stability of Cu-Mn/Zeolite Catalysts. *J. Phys. Chem. C* **2017**, *122*, 455–464. [[CrossRef](#)]
30. Liu, B.; Zhou, R.; Bu, N.; Wang, Q.; Zhong, S.; Wang, B.; Hidetoshi, K. Room-temperature ionic liquids modified zeolite SSZ-13 membranes for CO₂/CH₄ separation. *J. Membr. Sci.* **2017**, *524*, 12–19. [[CrossRef](#)]
31. Wang, D.; Gao, F.; Peden, C.H.F.; Li, J.; Kamasamudram, K.; Epling, W.S. Selective Catalytic Reduction of NO_x with NH₃ over a Cu-SSZ-13 Catalyst Prepared by a Solid-State Ion-Exchange Method. *ChemCatChem* **2014**, *6*, 1579–1583. [[CrossRef](#)]
32. Ye, Y.; Shen, F.; Wang, H.; Chen, R. SSZ-13-supported manganese oxide catalysts for low temperature selective catalytic reduction of NO_x by NH₃. *J. Chem. Sci.* **2017**, *129*, 765–774. [[CrossRef](#)]
33. Li, J.; Chang, H.; Ma, L.; Hao, J.; Yang, R.T. Low-temperature selective catalytic reduction of NO_x with NH₃ over metal oxide and zeolite catalysts—A review. *Catal. Today* **2011**, *175*, 147–156. [[CrossRef](#)]
34. Shan, W.; Song, H. Catalysts for the selective catalytic reduction of NO_x with NH₃ at low temperature. *Catal. Sci. Technol.* **2015**, *5*, 4280–4288. [[CrossRef](#)]
35. Gao, F.; Walter, E.D.; Kollar, M.; Wang, Y.; Szanyi, J.; Peden, C.H.F. Understanding ammonia selective catalytic reduction kinetics over Cu/SSZ-13 from motion of the Cu ions. *J. Catal.* **2014**, *319*, 1–14. [[CrossRef](#)]
36. Gao, F.; Mei, D.; Wang, Y.; Szanyi, J.; Peden, C.H.F. Selective Catalytic Reduction over Cu/SSZ-13: Linking Homo- and Heterogeneous Catalysis. *J. Am. Chem. Soc.* **2017**, *139*, 4935–4942. [[CrossRef](#)] [[PubMed](#)]
37. Janssens, T.V.W.; Falsig, H.; Lundegaard, L.F.; Vennestrøm, P.N.R.; Rasmussen, S.B.; Moses, P.G.; Giordanino, F.; Borfecchia, E.; Lomachenko, K.A.; Lamberti, C.; et al. A Consistent Reaction Scheme for the Selective Catalytic Reduction of Nitrogen Oxides with Ammonia. *ACS Catal.* **2015**, *5*, 2832–2845. [[CrossRef](#)]
38. Bates, S.A.; Delgass, W.N.; Ribeiro, F.H.; Miller, J.T.; Gounder, R. Methods for NH₃ titration of Brønsted acid sites in Cu-zeolites that catalyze the selective catalytic reduction of NO_x with NH₃. *J. Catal.* **2014**, *312*, 26–36. [[CrossRef](#)]
39. Zhu, H.; Kwak, J.H.; Peden, C.H.F.; Szanyi, J. In situ DRIFTS-MS studies on the oxidation of adsorbed NH₃ by NO_x over a Cu-SSZ-13 zeolite. *Catal. Today* **2013**, *205*, 16–23. [[CrossRef](#)]
40. Lezcano-Gonzalez, I.; Deka, U.; Arstad, B.; Van Yperen-De Deyne, A.; Hemelsoet, K.; Waroquier, M.; Van Speybroeck, V.; Weckhuysen, B.M.; Beale, A.M. Determining the storage, availability and reactivity of NH₃ within Cu-Chabazite-based Ammonia Selective Catalytic Reduction systems. *Phys. Chem. Chem. Phys.* **2014**, *16*, 1639–1650. [[CrossRef](#)]

41. Xie, L.; Liu, F.; Shi, X.; Xiao, F.-S.; He, H. Effects of post-treatment method and Na co-cation on the hydrothermal stability of Cu-SSZ-13 catalyst for the selective catalytic reduction of NO_x with NH₃. *Appl. Catal. B Environ.* **2015**, *179*, 206–212. [[CrossRef](#)]
42. Gao, F.; Szanyi, J. On the hydrothermal stability of Cu/SSZ-13 SCR catalysts. *Appl. Catal. A Gen.* **2018**, *560*, 185–194. [[CrossRef](#)]
43. Wang, J.; Zhao, H.; Haller, G.; Li, Y. Recent advances in the selective catalytic reduction of NO_x with NH₃ on Cu-Chabazite catalysts. *Appl. Catal. B Environ.* **2017**, *202*, 346–354. [[CrossRef](#)]
44. Paolucci, C.; Parekh, A.A.; Khurana, I.; Di Iorio, J.R.; Li, H.; Albarracin Caballero, J.D.; Shih, A.J.; Anggara, T.; Delgass, W.N.; Miller, J.T.; et al. Catalysis in a Cage: Condition-Dependent Speciation and Dynamics of Exchanged Cu Cations in SSZ-13 Zeolites. *J. Am. Chem. Soc.* **2016**, *138*, 6028–6048. [[CrossRef](#)]
45. Kwak, J.H.; Tran, D.; Burton, S.D.; Szanyi, J.; Lee, J.H.; Peden, C.H.F. Effects of hydrothermal aging on NH₃-SCR reaction over Cu/zeolites. *J. Catal.* **2012**, *287*, 203–209. [[CrossRef](#)]
46. Paolucci, C.; Verma, A.A.; Bates, S.A.; Kispersky, V.F.; Miller, J.T.; Gounder, R.; Delgass, W.N.; Ribeiro, F.H.; Schneider, W.F. Isolation of the Copper Redox Steps in the Standard Selective Catalytic Reduction on Cu-SSZ-13. *Angew. Chem. Int. Ed.* **2014**, *53*, 11828–11833. [[CrossRef](#)]
47. Gao, F.; Kwak, J.H.; Szanyi, J.; Peden, C.H.F. Current Understanding of Cu-Exchanged Chabazite Molecular Sieves for Use as Commercial Diesel Engine DeNO_x Catalysts. *Top. Catal.* **2013**, *56*, 1441–1459. [[CrossRef](#)]
48. Gao, F.; Wang, Y.; Kollár, M.; Washton, N.M.; Szanyi, J.; Peden, C.H.F. A comparative kinetics study between Cu/SSZ-13 and Fe/SSZ-13 SCR catalysts. *Catal. Today* **2015**, *258*, 347–358. [[CrossRef](#)]
49. Verma, A.A.; Bates, S.A.; Anggara, T.; Paolucci, C.; Parekh, A.A.; Kamasamudram, K.; Yezerets, A.; Miller, J.T.; Delgass, W.N.; Schneider, W.F.; et al. NO oxidation: A probe reaction on Cu-SSZ-13. *J. Catal.* **2014**, *312*, 179–190. [[CrossRef](#)]
50. Borfecchia, E.; Lomachenko, K.A.; Giordanino, F.; Falsig, H.; Beato, P.; Soldatov, A.V.; Bordiga, S.; Lamberti, C. Revisiting the nature of Cu sites in the activated Cu-SSZ-13 catalyst for SCR reaction. *Chem. Sci.* **2015**, *6*, 548–563. [[CrossRef](#)]
51. Ma, L.; Cheng, Y.; Cavataio, G.; McCabe, R.W.; Fu, L.; Li, J. In situ DRIFTS and temperature-programmed technology study on NH₃-SCR of NO_x over Cu-SSZ-13 and Cu-SAPO-34 catalysts. *Appl. Catal. B Environ.* **2014**, *156–157*, 428–437. [[CrossRef](#)]
52. Luo, J.; Gao, F.; Kamasamudram, K.; Currier, N.; Peden, C.H.F.; Yezerets, A. New insights into Cu/SSZ-13 SCR catalyst acidity. Part I: Nature of acidic sites probed by NH₃ titration. *J. Catal.* **2017**, *348*, 291–299. [[CrossRef](#)]
53. Kovarik, L.; Washton, N.M.; Kukkadapu, R.; Devaraj, A.; Wang, A.; Wang, Y.; Szanyi, J.; Peden, C.H.F.; Gao, F. Transformation of Active Sites in Fe/SSZ-13 SCR Catalysts during Hydrothermal Aging: A Spectroscopic, Microscopic, and Kinetics Study. *ACS Catal.* **2017**, *7*, 2458–2470. [[CrossRef](#)]
54. Han, L.; Zhao, X.; Yu, H.; Hu, Y.; Li, D.; Sun, D.; Liu, M.; Chang, L.; Bao, W.; Wang, J. Preparation of SSZ-13 zeolites and their NH₃-selective catalytic reduction activity. *Microporous Mesoporous Mater.* **2018**, *261*, 126–136. [[CrossRef](#)]
55. Fan, C.; Chen, Z.; Pang, L.; Ming, S.; Zhang, X.; Albert, K.B.; Liu, P.; Chen, H.; Li, T. The influence of Si/Al ratio on the catalytic property and hydrothermal stability of Cu-SSZ-13 catalysts for NH₃-SCR. *Appl. Catal. A Gen.* **2018**, *550*, 256–265. [[CrossRef](#)]
56. Gao, F.; Washton, N.M.; Wang, Y.; Kollár, M.; Szanyi, J.; Peden, C.H.F. Effects of Si/Al ratio on Cu/SSZ-13 NH₃-SCR catalysts: Implications for the active Cu species and the roles of Brønsted acidity. *J. Catal.* **2015**, *331*, 25–38. [[CrossRef](#)]
57. Leistner, K.; Kumar, A.; Kamasamudram, K.; Olsson, L. Mechanistic study of hydrothermally aged Cu/SSZ-13 catalysts for ammonia-SCR. *Catal. Today* **2018**, *307*, 55–64. [[CrossRef](#)]
58. Proding, S.; Derewinski, M.A.; Wang, Y.; Washton, N.M.; Walter, E.D.; Szanyi, J.; Gao, F.; Wang, Y.; Peden, C.H.F. Sub-micron Cu/SSZ-13: Synthesis and application as selective catalytic reduction (SCR) catalysts. *Appl. Catal. B Environ.* **2017**, *201*, 461–469. [[CrossRef](#)]

